Spin motive force driven by skyrmion dynamics in magnetic nanodisks

Yuhki Shimada* and Jun-ichiro Ohe
Department of Physics, Toho University, 2-2-1 Miyama, Funabashi, Chiba, Japan
(Received 10 December 2014; revised manuscript received 14 April 2015; published 28 May 2015)

The spin motive force driven by the dynamics of the skyrmion structure formed in a nanomagnetic disk is numerically investigated. Due to the existence of the magnetic structure along the disk edge, the collective mode of the magnetization is modified from that of the bulk skyrmion lattice obtained by using the periodic boundary condition. For a single-skyrmion disk, the dynamics of the skyrmion core and the edge magnetization induce the spin motive force, and a measurable AC voltage is obtained by two probes on the disk. For a multi-skyrmions disk, the phase-locked collective mode of skyrmions is found in the lowest resonant frequency where the amplitude of the AC voltage is enhanced by the cascade effect of the spin motive force. We also investigate the effect of the Rashba spin-orbit coupling on the spin motive force.

DOI: 10.1103/PhysRevB.91.174437 PACS number(s): 85.75.−d, 76.50.+g, 75.10.Hk, 75.78.−n

I. INTRODUCTION

Since 2010, the magnetic skyrmion lattice structure, a nontrivial topological excitation realized in helimagnetic materials such as MnSi, $Fe_{0.5}Co_{0.5}Si$, and CoO_2SeO_3, has been observed in real space [1], and the exploration of its physical properties has been carried out [2–14]. Skyrmion appears in the material by applying an external magnetic field and the competition between the Heisenberg coupling and Lifshitz invariants derived from the distortion of the crystal structure. This is configured by the local magnetization filling the solid angle of all; in other words, it is a particlelike topological structure with the winding number one [15]. Thanks to the quantized geometric nature, the structure withstands against moderate perturbations [2,3]. Due to the topological charge, this magnetic texture shows the topological Hall effect [14,16]. The method of generation/annihilation and the drive by ultra-low current density are also reported [4–7]. The structure also has the vector chirality, resulting in the nature multiferroics [8]. From its characteristics and diverse physical properties as mentioned above, the skyrmion structure has attracted attention not only as a subject of fundamental physics but also its potential of information bits in next generation spintronics devices.

Recently, it has been pointed out that the dynamics of the nonuniform magnetization structure in a metallic sample gives an effective field acting on the conduction electrons. The effective field, called spin motive force, is understood in terms of the spin Berry's phase that corresponds to the solid angle of spinor in the SU(2) space [17–19]. This force results from the magnetization dynamics represented by [19,20]

$$E_\mu = \frac{\hbar}{2e}\mathbf{m}\cdot(\partial_\mu\mathbf{m}\times\partial_t\mathbf{m}) + E^{\mathrm{R}}_\mu(\alpha_{\mathrm{R}}),\ (\mu = x, y, z), \quad (1)$$

where $\hbar = h/2\pi$, e, and $\mathbf{m} = \mathbf{M}/M_{\mathrm{s}}$ are Plank's constant, elementary charge, and the direction of the magnetization, respectively. M_{s} is the saturation magnetization. The second term of Eq. (1) is the spin motive force due to Rashba spin-orbit interaction $\mathbf{E}^{\mathrm{R}}(\alpha_{\mathrm{R}}) = \alpha_{\mathrm{R}}\frac{m_e}{e\hbar}(\hat{\mathbf{z}}\times\partial_t\mathbf{m})$, where α_{R} is the Rashba parameter, and m_e is the electron mass [21]. Without Rashba spin-orbit interaction ($\alpha_{\mathrm{R}} = 0$), the amplitude of the spin motive force is proportional to the spatiotemporal derivative of the magnetization, and one can expect the large spin motive force can be induced by the dynamics of the skyrmion structure. The collective mode of the skyrmion lattice has been studied by Mochizuki for bulk systems where the periodic boundary condition is employed [9]. They found the counterclockwise (CCW) and clockwise (CW) collective mode by applying the in-plane AC field to the skyrmion lattice. For these modes, the skyrmion core rotates around the quasilattice point forming the close-packed structure. By applying the out-of-plane field, the breathing mode, the repeating mode of expansion and contraction of the skyrmion core, is excited. Ohe shows that the spin motive force driven by the CCW and CW modes induces the measurable voltage by using the bulk sample [10]. In order to use the skyrmion in actual devices, an isolated sample should be treated in which the collective mode is modulated by the magnetization structure around the sample edge.

In this paper, we numerically investigate the spin motive force driven by the dynamics of the skyrmion created in a magnetic nanodisk. In contrast to the skyrmion dynamics of the bulk sample obtained by the periodic boundary condition, the collective mode of the magnetization shows the coupling between the motion of the skyrmion inside the sample and the motion of the edge structure constituted along the sample edge. We prepare the single- and multi-skyrmion disk for investigating the size effect. For a single-skyrmion disk, the spectrum calculation reveals four collective modes are generated by coupling between the rotating mode of the skyrmion and the rotating mode of the edge structure. Calculated spin motive force is of the order of 1 V/m for each mode, and the measurable voltage is 30 nV at the lowest resonant frequency mode for a disk with a diameter of 20 nm. For a multi-skyrmion disk, the collective mode shows a complex dynamics in contrast to that obtained by the bulk system and the single-skyrmion disk. The spectrum peak is broadened because of the coupling between the skyrmions and the edge. We found that the phase-locked motion of each skyrmion is only obtained in the lowest frequency mode. The voltage signal is enhanced by the cascade effect of the spin motive force in the lowest frequency mode. Obtained results reveal that the collective mode of the skyrmion lattice in an isolated disk

*7415001s@nc.toho-u.ac.jp

is different from that of the bulk sample. Furthermore, we investigate the effect of the Rashba spin-orbit coupling due to the lack of inversion symmetry in a thin film. The amplitude and the direction of the spin motive force are modified by the Rashba spin-orbit interaction. Numerical results show the measurable voltage is enhanced by the spin-orbit interaction, and the phase shift of the AC voltage occurs. The obtained results give the possibility of a new type of spin battery for utilizing skyrmion structure.

II. MODEL AND METHOD

The effective Hamiltonian of a chiral magnet is represented by [9,10,16]

$$\begin{aligned}\mathcal{H} = &-J\sum_{\langle i,j\rangle}\mathbf{m}_i\cdot\mathbf{m}_j \\ &+D\sum_i[(\mathbf{m}_i\times\mathbf{m}_{i+a\hat{\mathbf{x}}})_x+(\mathbf{m}_i\times\mathbf{m}_{i+a\hat{\mathbf{y}}})_y] \\ &-VM_s[\mathbf{B}^{\mathrm{DC}}+\mathbf{B}^{\mathrm{AC}}(t)]\cdot\sum_i\mathbf{m}_i, \end{aligned} \tag{2}$$

where V, $\mathbf{B}^{\mathrm{DC}}$, $\mathbf{B}^{\mathrm{AC}}(t)$, and a are volume of unit cell, static magnetic field, oscillating magnetic field, and lattice constant, respectively. The ratio between the exchange coupling energy J and the Dzyaloshinskii-Moriya coupling energy D is an important parameter that determines the core size of the skyrmion on the ground state. We set $D/J = 0.5$, then the pitch of the helix structure is ≈8.5 nm [14]. The dynamics of the localized magnetization at site i obeys the Landau-Lifshitz-Gilbert-Slonczewski equation [22]

$$\partial_t\mathbf{m}_i = -|\gamma|\mathbf{m}_i\times\mathbf{B}_i^{\mathrm{eff}}+\alpha\mathbf{m}_i\times\partial_t\mathbf{m}_i+\boldsymbol{\tau}, \tag{3}$$

where gyromagnetic ratio is $\gamma = -1.76\times10^{11}$ Hz/T, and the Gilbert damping coefficient is $\alpha = 0.01$. The third term of the right-hand side of Eq. (3) is the spin transfer torque $\boldsymbol{\tau} = \frac{\gamma\hbar}{2eM_s}(\mathbf{j}\cdot\nabla)\mathbf{m}$ ($\mathbf{j}$ is spin current density) due to the current induced by the spin motive force. In this paper, we found that the charge current density of the spin motive force is much smaller than that which induces the skyrmion motion, therefore we neglect this spin transfer torque term. The effective magnetic field is given by $\mathbf{B}_i^{\mathrm{eff}} = -\frac{1}{V}\frac{\partial\mathcal{H}}{\partial\mathbf{M}_i}$. We employ the parameters of MnSi film [14], and the thickness of the sample is 10 nm. According to the transition temperature of the experiment on MnSi, the exchange coupling constant is $J/k_{\mathrm{B}} = 45$ K where k_{B} is the Boltzmann constant. To perform the numerical simulations, we use the two-dimensional square lattice consisting of unit cell $0.5\times0.5\times10$ nm^3. We employ the fourth-order Runge-Kutta method for calculating the time evolution of Eq. (3), and a time step is 1 ps. The spin motive force is calculated by the magnetization dynamics by using Eq. (1). In order to calculate the measurable voltage, we solve the Poisson equation $\nabla^2\phi_i = -\nabla\cdot\mathbf{E}_i$ that gives the potential configuration ϕ_i in the sample. We assume that two probes put on the system as shown in Fig. 1(a). The voltage difference between two probes is defined by $\Delta V \equiv \langle\sum'_{i\in(i_x<5\text{ nm})}\phi_i\rangle - \langle\sum'_{i\in(i_x>d-5\text{ nm})}\phi_i\rangle$, where d is the diameter of the sample, $\sum'$ runs only the probe area, and $\langle\cdots\rangle$ represents the average.

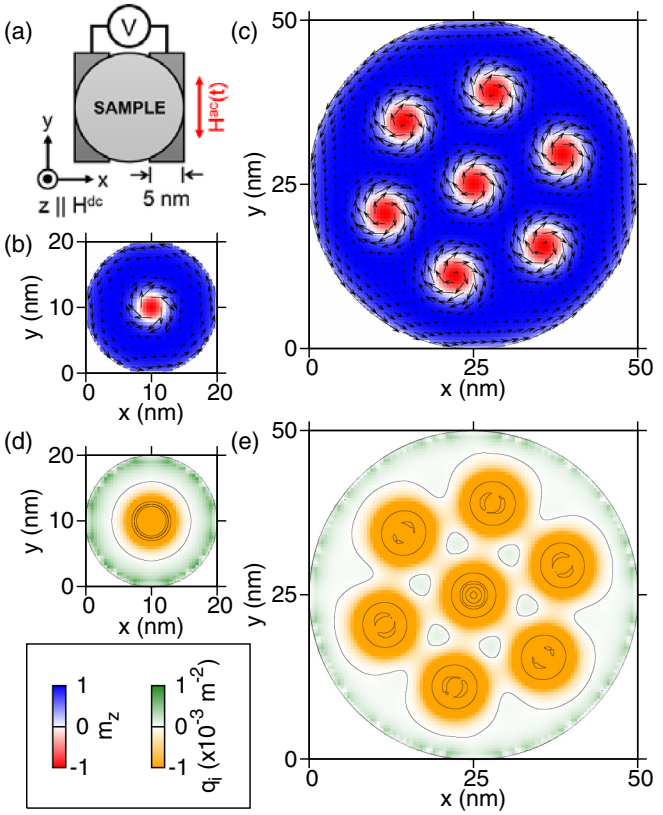

FIG. 1. (Color online) (a) The schematic view of the calculated system. Two probes are set on the disk edge and the width is 5 nm. (b),(c) The ground state configuration of the magnetization at $B^{\mathrm{DC}} = 26$ mT in real space. Each arrow represents the in-plane component of local magnetization. (b) and (c) indicates the single- and multi-skyrmion disk, respectively. (d),(e) The topological charge density of each disk.

III. NUMERICAL RESULTS AND DISCUSSIONS

A. Without spin-orbit interaction ($\alpha_{\mathrm{R}} = 0$)

First, we show the ground state of the magnetic structure with the out-of-plane static field $B^{\mathrm{DC}} = 26$ mT in Figs. 1(b)–1(e). We use the diameter of the nanodisk $d = 20$ nm [Fig. 1(b)] and 50 nm [Fig. 1(c)] in which the magnetization forms a single skyrmion and seven skyrmions, respectively. The skyrmion core sets a close-packed structure inside the disk as well as the bulk sample. On the other hand, one can see the additional structure along the edge of the disk. Such a chiral magnetization structure is characterized by the topological charge defined as $q_i = (1/4\pi)\mathbf{m}_i\cdot\left(\partial_x\mathbf{m}_i\times\partial_y\mathbf{m}_i\right)$. Figures 1(d) and 1(d) show the topological charge density for each disk. The positive value of the charge appears around the edge of the disk, while the negative value appears near the skyrmion core. This additional edge structure gives an additional collective mode in the magnetic dynamics. Both the skyrmion and the edge are moved by applying the in-plane magnetic field. From Eq. (1), one can estimate the generating spin motive force driven by the dynamics of the topological charge as

$$E_\mu = \frac{\hbar}{2e}v_\nu(\partial_\nu\mathbf{m}\times\partial_\mu\mathbf{m})\cdot\mathbf{m}, \tag{4}$$

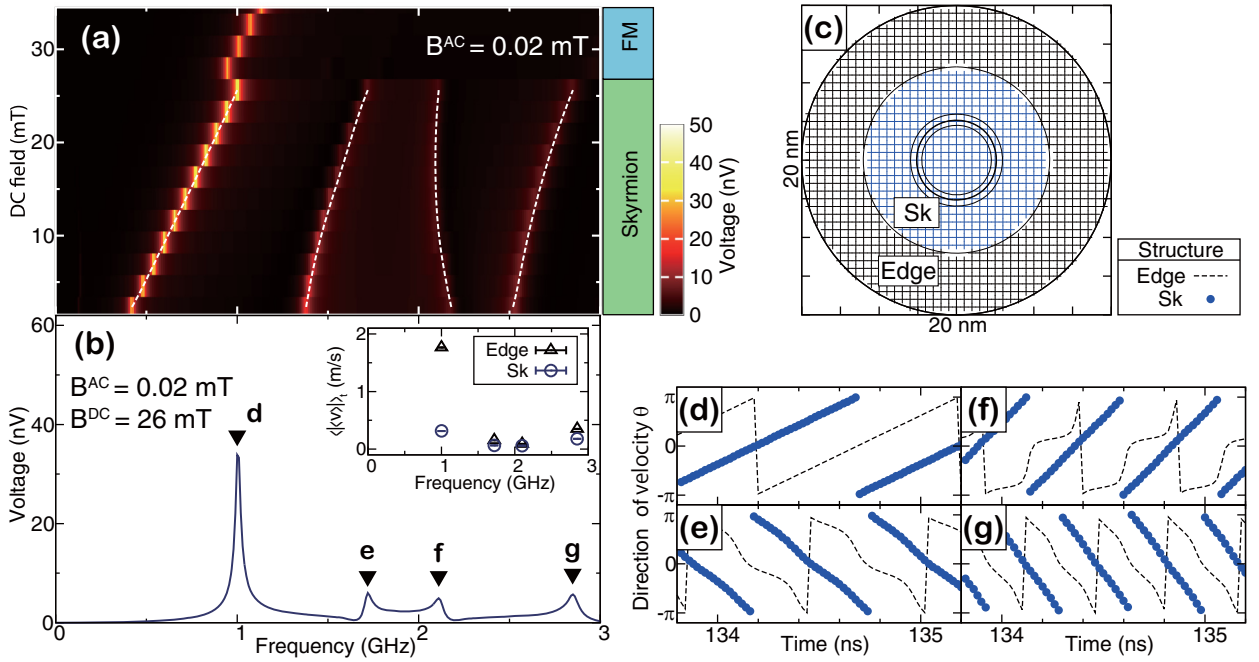

FIG. 2. (Color online) The results of the single-skyrmion disk without Rashba spin-orbit interaction. (a) The magnitude of AC voltage signal as a function of the static field and the frequency. (b) The frequency dependence of the voltage and of the time averaged magnitude of the topological charge velocity in Eq. (4) (inset) with $B^{\mathrm{DC}} = 26$ mT. (c) Each structure region for analyzing the velocity. The contours are comparable to Fig. 1(d). (d)–(g) The direction of velocity defined by $\theta(t) = \tan^{-1}(\frac{\langle v_y \rangle}{\langle v_x \rangle}) - \frac{\langle v_x \rangle}{|\langle v_x \rangle|}$ at each resonant mode, where $\langle \cdots \rangle$ is averaged over the region of each structure (c).

where v_ν ($\nu = x, y, z$) is the velocity of the topological charge. The direction of the spin motive force is perpendicular to the velocity of the magnetic structure in the two-dimensional system. The edge structure also induces the spin motive force, the direction of which is determined by the motion of the topological charge. Especially when the frequency of the magnetic field corresponds to the resonant frequency of the system, the large spin motive force is induced. We will point out that the resonant mode of the skyrmion disk is formed both from the dynamics of the skyrmion and the edge structure.

Figure 2(a) shows the voltage between two probes as a function of the static field and the frequency of in-plane AC field for the single-skyrmion disk. By increasing the static field, the magnetic structure shows the phase transition from the skyrmion phase to the ferromagnetic (FM) phase at 28 mT. In the skyrmion phase $B_z^{\mathrm{DC}} \leqslant 28$ mT, four resonant peaks are obtained although two modes (CW and CCW) are obtained in the bulk system mentioned in previous papers [9,10]. From the motion of the structures, we clarify that the origin of the additional peak comes from the coupling between the skyrmion core motion and the edge resonant motion. For the isolated disk, the collective mode is characterized not only by the motion of the skyrmion core but also by the resonant motion of the edge. Figures 2(d)–2(g) show the angle of the velocity of the topological charge derived from Eq. (4) for the skyrmion and the edge structure. We divide the area of the skyrmion and the edge as shown in Fig. 2(c), and the average of the velocity is calculated for each area. Figures 2(d) and 2(f) indicate the CCW mode is excited while Figs. 2(e) and 2(g) indicate the CW mode is excited in each frequency. For each resonant state, the amplitude of the spin motive force become large both near the skyrmion core and the edge. When we set the static field with 26 mT, the voltage difference shows maximum value at $f = 1.0$ GHz as shown in Fig. 2(b). For this resonant mode, the spin motive force becomes large ($\geqslant$1 V/m) in the whole sample. For other higher resonant modes, such a large spin motive force is generated in a narrow region both at the skyrmion and the disk edge because the magnitude of the topological charge velocity in Eq. (4) is restrained [see Fig. 2(b)] although the nonuniform structures have large spatial derivative. This causes the small voltage difference on two probes compared to the lowest mode. We note that the voltage difference is also observed in the FM region ($B^{\mathrm{DC}} \geqslant 28$ mT). This spin motive force is caused by the dynamics of the edge magnetization structure that survives despite the vanishing of the skyrmion structure.

For a multi-skyrmion disk, the number of the resonant mode increases from that of a single-skyrmion disk as shown in Fig. 3(a). The resonant mode is formed from the rotating of the skyrmion core and the resonant state of the edge as well as the single-skyrmion disk. The coupling between individual skyrmions makes the resonant mode complex. From Fig. 3(b), the large voltage difference is obtained in the lowest resonant frequency mode [labeled **d** in Fig. 3(b)]. We clarify that this large voltage difference originates from the cascade effect of the spin motive force as well as a bulk case [10]. Figures 3(d)–3(g) show the phase of motion for individual structures in the disk at each resonant mode labeled in Fig. 3(b), and the motion is analyzed using the same method as Figs. 2(d)–2(g) where the calculated region for each structure is shown in Fig. 3(c). Figure 3(d) shows the phase-locked motion of skyrmions and the spin motive force points the same direction

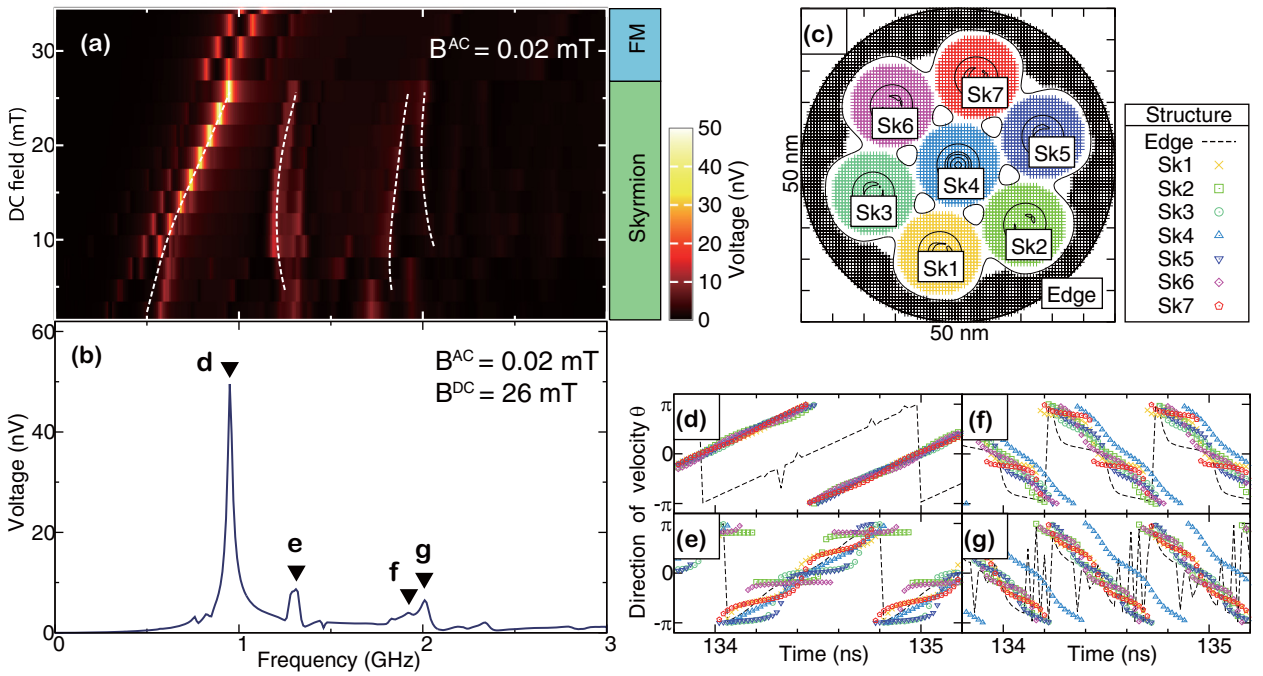

FIG. 3. (Color online) The results of multi-skyrmion disk without Rashba spin-orbit interaction. The plot conditions are the same as Fig. 2.

for each skyrmion at any moment. For other resonant motions [Figs. 3(e)–3(g)], however, the spin motive force of each skyrmion does not point in the same direction. Especially in the higher two modes, the dynamics of the skyrmion at the center is quite different from that of the skyrmion near the edge. This disturbance causes the suppression of the cascade effect of the spin motive force. When the spin motive force points in the same direction for each skyrmion, the voltage difference becomes large because of the cascade effect [10]. Therefore, we found that this cascade effect appears only when the lowest resonant frequency mode is excited. For the bulk sample, it has been pointed out that the amplitude of the AC voltage is proportional to the number of the skyrmion between two probes. For the isolated disk system, an open boundary condition reduces the voltage potential near the sample edge. In Fig. 4, we show the voltage as a function of time for the single- and multi-skyrmion systems. One can see that the amplitude of the AC voltage becomes large by increasing the number of the skyrmion. From the results of the multi-skyrmion disk, we can estimate the voltage is of the order of 10 μV when the diameter of the disk is $\sim$50 μm including a few thousand skyrmions. We note that the breathing mode shows a point symmetric structure that cannot generate the voltage difference in the present setup.

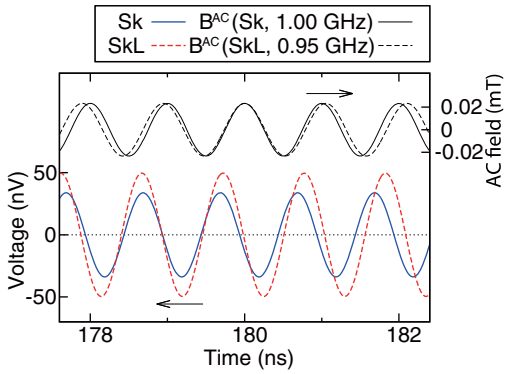

FIG. 4. (Color online) (Lower curves) The voltage as a function of the time. (Upper curves) The in-plane oscillating field. Each frequency of the field is $f = 1.00$ GHz (single-skyrmion disk) and 0.95 GHz (multi-skyrmion disk).

B. With spin-orbit interaction ($\alpha_R \neq 0$)

Next, we consider the presence of the Rashba spin-orbit interaction for a two-dimensional thin film and set the Rashba parameter $\alpha_R = 10^{-10}$ eV m in Eq. (1). In Figs. 5(a) and 5(b), we compare the spin motive force in real space with and without the spin-orbit interaction. One can see that the magnitude of the spin motive force is ten times larger when the Rashba spin-orbit interaction exists.

From Eq. (1), the direction of the spin motive force is also modulated. We show the time dependence of the voltage in Fig. 5(c). We obtained the cascade effect even in the presence of the Rashba spin-orbit interaction despite the signal phase shift occurring [Fig. 5(c)]. The amplitude of AC voltage signal becomes larger than the case without the spin-orbit interactions which reaches to 180 nV.

IV. CONCLUSION

We have numerically studied the spin motive force driven by the skyrmion structure created in a magnetic nanodisk. The collective mode is modulated from that of the bulk mode because of the resonant motion of the edge magnetization. The in-plane oscillating field excites four collective modes in a single-skyrmion disk. These collective modes can be understood in terms of the coupling between counterclockwise

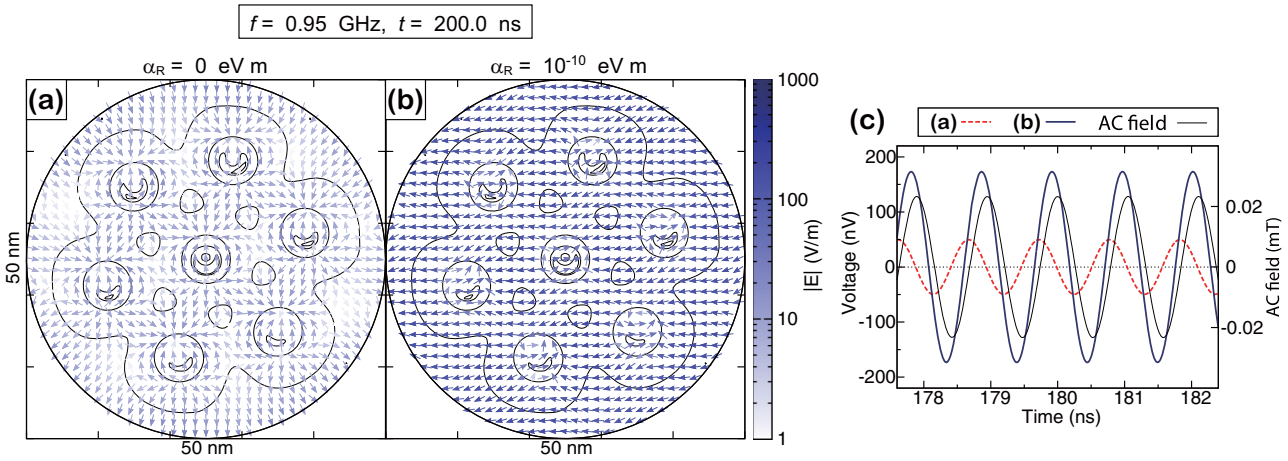

FIG. 5. (Color online) The snapshots of spin motive force with lowest resonant mode in multi-skyrmion disk. (a),(b) There are contours of topological charge. Arrows represent the direction of spin motive force and the color gradient shows the magnitude. (a) is an ordinary case without Rashba spin-orbit interaction ($\alpha_R = 0$ eV m). (b) With Rashba effect ($\alpha_R = 10^{-10}$ eV m). (c) Comparing the voltage signal of both cases (a) and (b).

mode and clockwise mode at the skyrmion and resonant mode of the edge. For a multi-skyrmion disk, the resonant peaks are broadened because of the coupling between each skyrmion motion. The phase-locked motion is obtained only in the lowest resonant frequency mode. The measurable voltage increases by increasing the number of the skyrmion due to the cascade effect of the spin motive force in this lowest frequency mode. Our numerical results show that the cascade effect is not obtained in higher frequency modes because the direction of the spin motive force is not synchronized in each skyrmion. The result in the presence of the Rashba spin-orbit coupling reveals the increasing of the cascaded spin motive force signal and the phase shift of the AC voltage. The skyrmion based technology has attracted much attention recently, and our proposed mechanism may provide the small battery in spintronics devices.

[1] X. Z. Yu, Y. Onose, N. Kanazawa, J. H. Park, J. H. Han, Y. Matui, N. Nagaosa, and Y. Tokura, Nature (London) **465**, 901 (2010).

[2] X. Z. Yu, N. Kanazawa, Y. Onose, K. Kimoto, W. Z. Zhang, S. Ishiwata, Y. Matsui, and Y. Tokura, Nat. Mater. **10**, 106 (2011).

[3] M. Mochizuki, X. Z. Yu, S. Seki, N. Kanazawa, W. Koshibae, J. Zang, M. Mostovoy, Y. Tokura, and N. Nagaosa, Nat. Mater. **13**, 241 (2014).

[4] F. Jonietz, S. Mühlbauer, C. Pfleiderer, A. Neubauer, W. Münzer, A. Bauer, T. Adams, R. Georgii, P. Böni, R. A. Duine, K. Everschor, M. Garst, and A. Rosch, Science **330**, 1648 (2010).

[5] X. Z. Yu, N. Kanazawa, W. Z. Zhang, T. Nagai, T. Hara, K. Kimoto, Y. Matsui, Y. Onose, and Y. Tokura, Nat. Commun. **3**, 988 (2012).

[6] J. Iwasaki, M. Mochizuki, and N. Nagaosa, Nat. Nanotech. **8**, 742 (2013).

[7] J. Iwasaki, M. Mochizuki, and N. Nagaosa, Nat. Commun. **4**, 1463 (2013).

[8] M. Mochizuki and S. Seki, Phys. Rev. B **87**, 134403 (2013).

[9] M. Mochizuki, Phys. Rev. Lett. **108**, 017601 (2012).

[10] J. Ohe and Y. Shimada, Appl. Phys. Lett. **103**, 242403 (2013).

[11] Y. Onose, Y. Okamura, S. Seki, S. Ishiwata, and Y. Tokura, Phys. Rev. Lett. **109**, 037603 (2012).

[12] K. Everschor, M. Garst, B. Binz, F. Jonietz, S. Muhlbauer, C. Pfleiderer, and A. Rosch, Phys. Rev. B **86**, 054432 (2012).

[13] Naoto Nagaosa and Yoshinori Tokura, Nat. Nanotech. **8**, 899 (2013).

[14] Y. Li, N. Kanazawa, X. Z. Yu, A. Tsukazaki, M. Kawasaki, M. Ichikawa, X. F. Jin, F. Kagawa, and Y. Tokura, Phys. Rev. Lett. **110**, 117202 (2013).

[15] A. N. Bogdanov and D. A. Yablonskii, Zh. Eksp. Teor. Fiz. **95**, 178 (1989) [Sov. Phys. JETP **68**, 101 (1989)].

[16] S. D. Yi, S. Onoda, N. Nagaosa, and J. H. Han, Phys. Rev. B **80**, 054416 (2009).

[17] A. Stern, Phys. Rev. Lett. **68**, 1022 (1992).

[18] S. E. Barnes and S. Maekawa, Phys. Rev. Lett. **98**, 246601 (2007).

[19] G. E. Volovik, J. Phys. C **20**, L83 (1987).

[20] J. Ohe, S. E. Barnes, H.-W. Lee, and S. Maekawa, Appl. Phys. Lett. **95**, 123110 (2009).

[21] K.-W. Kim, J.-H. Moon, K.-J. Lee, and H.-W. Lee, Phys. Rev. Lett. **108**, 217202 (2012).

[22] A. Brataas, A. D. Kent, and H. Ohno, Nat. Mater. **11**, 372 (2012).